Nano Energy 39 (2017) 60–68

Contents lists available at ScienceDirect

Nano Energy

journal homepage: www.elsevier.com/locate/nanoen

Full paper

Humidity resistant fabrication of $CH_3NH_3PbI_3$ perovskite solar cells and modules

Joel Troughton, Katherine Hooper, Trystan M. Watson*

SPECIFIC, Swansea University Bay Campus, Fabian Way, Swansea SA1 8EN, United Kingdom

ARTICLE INFO

Keywords:
Perovskite
Humidity
Anti-solvent
Ethyl acetate
Module

ABSTRACT

A humidity resistant and versatile fabrication method for the production of very high quality, organic-inorganic perovskite films, solar cells and solar modules is presented. By using ethyl acetate as an anti-solvent during deposition, perovskite solar cells with power conversion efficiencies (PCEs) up to 15% were fabricated in a 75% relative humidity (RH) environment. Ethyl acetate acts as a moisture absorber during spin-coating, protecting sensitive perovskite intermediate phases from airborne water during film formation and annealing. We have demonstrated the manufacture of 50 mm × 50 mm series interconnected modules with PCEs in excess of 10% for 13.5 cm^2 devices processed in air at 75%RH and 11.8% at 50%RH. To the best of our knowledge, these results represent the highest efficiency for perovskite solar modules processed under high humidity ambient conditions. This new deposition protocol allows for low-cost, efficient and consistent device fabrication in humid climates and uncontrolled laboratories.

1. Introduction

Since the seminal work by Miyasaka in 2009 [1], followed by the move to fully solid-state devices in 2012 by the groups of Snaith [2] and Gratzel [3], metal halide perovskite solar cells (PSCs) have taken the photovoltaic (PV) research community by storm [4]. From humble power-conversion efficiencies (PCEs) of 3.8% at their inception [1], to current certified values in excess of 22% [5], the technology now rivals incumbent thin-film technologies such as CdTe and $Cu(InGa)Se_2$. The high performance of PSCs may be attributed to the perovskite absorber's excellent electronic [6] and optical properties, both of which may be tuned by varying the material's composition of organic or inorganic constituents [7].

One of the key differentiators for the rapid surge in interest regarding PSCs compared to other 3rd generation photovoltaic technologies is the ease of which such devices may be fabricated. Several routes to the deposition of a perovskite film have been developed including single-step spin-coating, sequential deposition of inorganic and organic components [8], thermal evaporation and vapor processing of components [9,10]. In addition, many different device structures exist, ranging from “normal”, or “n-i-p” structures with an electron transport layer closest to the substrate, to “inverted” or “p-i-n” structures where a hole transport layer is closest to the substrate [11,12]. Devices employing the normal structure may also incorporate a mesoporous scaffold network of nanoparticles, typically TiO_2 to act as a large surface area photoanode, whereas inverted devices tend to be fully planar in nature.

While PSCs hold many advantages compared to other PV technologies, one critical drawback is their sensitivity to moisture within the air both during processing and during their operational lifetime whereby the organic cation within the perovskite structure is typically dissolved by water [13–16]. As a result, the overwhelming majority of PSCs currently presented in literature are fabricated under highly controlled atmospheric conditions in order to maintain consistent and high performance levels. In the majority of cases, N_2-filled glove boxes are used with only trace levels of oxygen and water. This may pose a barrier to the eventual manufacture of PSCs, where large-scale stringent atmospheric control could prove financially prohibitive. There has been some admirable research in the area of processing perovskite films in air, although these studies tend to maintain relative humidity levels far lower than what may be experienced under true environmental conditions in certain climates [17–24]. However, this is not always the case as demonstrated in an article by Tai and coworkers [25], where efficient and highly stable PSCs were produced on mesoporous TiO_2 scaffolds at humidities in excess of 70%RH using a novel $Pb(SCN)_2$ precursor in a two-step deposition process. While the technique may prove limited in its application to other perovskite absorber materials and processing routines, the ability to produce devices at such high ambient humidity represents a step forward in the technology's eventual commercialization.

* Corresponding author.
E-mail address: T.M.Watson@swansea.ac.uk (T.M. Watson).

http://dx.doi.org/10.1016/j.nanoen.2017.06.039
Received 8 February 2017; Received in revised form 8 May 2017; Accepted 23 June 2017
Available online 24 June 2017

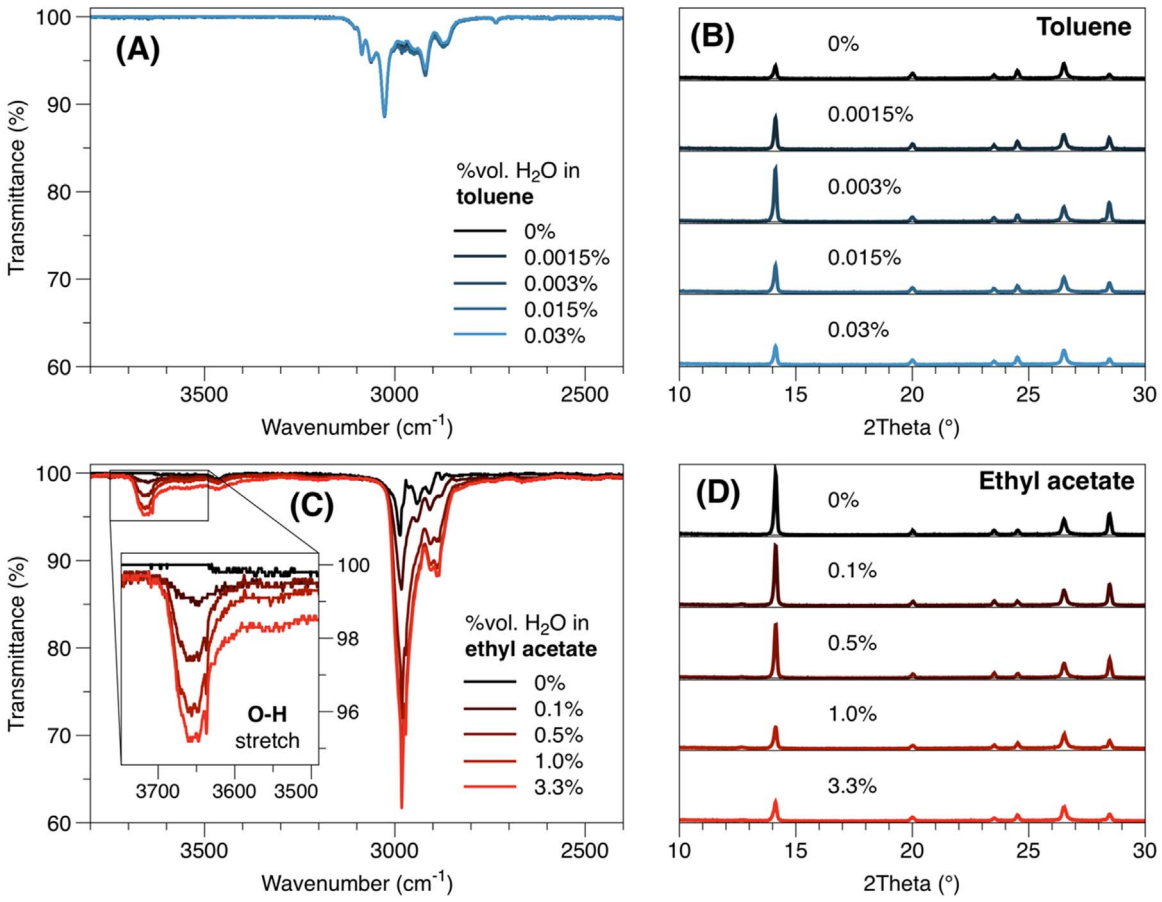

Fig. 1. (A) FTIR spectra of toluene with varying volumes of added H_2O. (B) XRD patterns of $CH_3NH_3PbI_3$ films processed at 40%RH with hydrated toluene anti-solvent dripping. (C) FTIR spectra of ethyl acetate with varying volumes of added H_2O. (B) XRD patterns of $CH_3NH_3PbI_3$ films processed at 40%RH with hydrated ethyl acetate anti-solvent dripping.

Here, we report a robust and repeatable method for depositing and annealing high quality perovskite films in very high humidity conditions using single step spin-coating. By modifying a popular anti-solvent single step spin-coating method to include an anti-solvent with a high scavenging affinity for moisture, ethyl acetate, we are able to produce perovskite films with consistent crystalline, morphological and electronic properties in environments ranging from 0%RH to 75%RH. Other popular anti-solvents were also compared including diethyl ether [26], toluene [27] and chlorobenzene [28–30] and were found to produce increasingly poor quality films as processing humidity is increased. This modified method is demonstrated to be applicable to multiple perovskite solar cell architectures including the "inverted"-type structures employing NiO and PCBM as charge selective layers, as well as in mesoporous "normal" structures using TiO_2 and spiro-OMeTAD. Using this method, hysteresis-free planar perovskite solar cells with PCEs of up to 14.5% were fabricated in 75%RH ambient air, with mesoporous structured devices reaching 15% PCE under the same conditions. The fabrication protocol also allows for highly uniform film deposition over large surface areas under these otherwise unfavorable environments, as demonstrated by 13.5 cm^2 module PCEs achieving 10.1% and 11.8% for 75%RH and 50%RH processing conditions respectively.

2. Results & discussion

Ethyl acetate (EA) has previously been reported as an anti-solvent for the rapid crystallization of $CH_3NH_3PbI_3$ perovskite in an article by Yin and coworkers [31], albeit in a controlled N_2 glovebox environment. During the spin-coating of a perovskite precursor in a solution containing dimethylsulfoxide (DMSO), a so-called "anti-solvent" which is miscible in the precursor solvents, but orthogonal to the perovskite itself is poured onto the spinning substrate. In the case of a typical anti-solvent such as toluene [27], this quenching washes much of the precursor solvent away and causes the formation of an intermediate phase comprising of MAI-PbI_2-DMSO. Upon heating, residual DMSO is removed and the perovskite film is formed from the remaining salts [27]. When a sufficient volume of ethyl acetate is used as an anti-solvent, the intermediate MAI- PbI_2-DMSO phase is eventually by-passed during the spin-coating process as a result of the anti-solvent fully removing DMSO from the film [31]. It is important to note, however, that if insufficient ethyl acetate is poured onto the spinning sample the intermedia phase will not be fully bypassed as evidenced by its pale appearance. To illustrate this, a photograph of a perovskite film immediately after having undergone a 200 µl ethyl acetate quenching treatment, as well as after annealing is shown in Fig. S1. The protection of this intermediate phase is crucial for high quality film formation under high humidity processing conditions owing to the reported instability of such a phase [32].

2.1. Characterization of perovskite films produced using hydrated anti-solvents

An interesting characteristic of ethyl acetate is its ability to dissolve a large amount of water (3.3 vol% of water) [33] compared to other commonly used anti-solvents such as diethyl ether (1.5%) [34], toluene (0.033%) [35] and chlorobenzene (0.04%) [36]. We propose that this affinity for moisture is largely responsible for ethyl acetate's improved performance in high humidity applications. Upon deposition of ethyl acetate onto the spinning perovskite precursor, moisture within the air is sequestered in solution with the anti-solvent rather than reacting

with the perovskite intermediate phase, as is the case in other anti-solvents with a reduced capacity to dissolve water. Consequently, perovskite films spin-coated using ethyl acetate as an anti-solvent exhibit highly uniform and smooth surfaces compared to other anti-solvents which are more prone to degradation from water during the spin-coating process. To support such a theory, solutions of anhydrous ethyl acetate and toluene were deliberately contaminated with varying concentrations of water and used during the fabrication of perovskite films.

Fig. 1 shows FTIR spectra of toluene (A) and ethyl acetate (C) solvents with varying amounts of added H_2O for comparison. The highest concentrations of water in solution correspond to the saturation limits for both solvents, with all solutions being mixed thoroughly before analysis to ensure dissolution. As expected, ethyl acetate exhibits a progressive deepening of the peak at 3650 cm^{-1} with increasing water concentrations, corresponding to the O-H bond within the molecule. By comparison, toluene is able to dissolve so little water (up to 0.033% by volume) [35] that the same region shows no difference between anhydrous and fully saturated. This demonstrates toluene's inability to absorb any significant volume of water from moist air, in comparison to ethyl acetate. In order to determine the impact of anti-solvent moisture content on perovskite film quality, layers of $CH_3NH_3PbI_3$ were processed in air (40%RH, 20 °C) using varyingly water saturated toluene and ethyl acetate as anti-solvents during spin-coating. X-ray diffraction (XRD) patterns for these films are seen in Fig. 1B and D for toluene and ethyl acetate respectively. Photographs of the resulting films are presented in Fig. S2.

In Fig. 1B and D, the crystalline nature of the perovskite material is confirmed in both cases, being identified as the tetragonal phase of $CH_3NH_3PbI_3$ (*I*4/*mcm*), based on XRD data previously reported by Baikie et al. [37]. All patterns shown in Fig. 1B and D have been normalized to the height of the peak at 26.5°, corresponding to the FTO present on the glass substrate. Peaks at 14.04° and 28.38° correspond to the (110) and (220) crystal planes within the perovskite film and serve as a metric for the material's crystallinity. Patterns from toluene-processed films indicate a slight increase in crystallinity when using an anti-solvent with 0.003 vol% added water, which may be a result of slightly improved grain formation when annealing in the presence of moisture [38]. Because of toluene's inability to absorb water, airborne moisture is allowed to interact with the perovskite intermediate phase during spin-coating leading to overall diminished (110) and (220) peaks in most films shown in Fig. 1B. On the other hand, films produced using ethyl acetate show excellent resistance to water contamination within the anti-solvent: At volume fractions up to 0.5%, minimal depression of the (110) and (220) peaks is observed compared to the anhydrous control, with larger decreases manifesting at 1.0% and 3.3% water loading. As a consequence of airborne moisture being trapped within the ethyl acetate during spin-coating instead of reacting with the perovskite intermediate phase, crystallinity of the resulting film remains high despite high ambient humidity during deposition and annealing. At water volume fractions greater than 1.0%, the ethyl acetate's ability to sequester water is diminished, resulting in more atmospheric moisture interaction with the perovskite, leading to poorer film quality.

2.2. Characterization of perovskite film quality through SEM imagery and XRD

Fig. 2 shows an image of $CH_3NH_3PbI_3$ films spin-coated and annealed in a 75% relative humidity environment in air using different anhydrous anti-solvents to aid film formation. The highly reflective nature of the film processed using ethyl acetate (Fig. 2A) is indicative of a continuous and pinhole-free layer. The films produced from diethyl ether, toluene and chlorobenzene anti-solvents (Fig. 2B, C and D respectively) show varying degrees of haziness on their surfaces indicating light-scattering pinholes and a rougher perovskite layer. Fig. 3 shows SEM micrographs of $CH_3NH_3PbI_3$ films produced using the different anti-solvents in environments with relative humidities of 0%, 30%, 50% and 75%. While the latter 3 humidity points were performed in air, 0%RH samples were processed in a N_2-filled glovebox.

It is immediately apparent from Fig. 3 that perovskite films processed within a N_2 glovebox exhibit largely the same morphological arrangement with grains ranging between 100 and 400 nm in diameter and no pinholes present. As films are fabricated under increasingly higher humidity environments, severe degradation occurs in chlorobenzene and toluene treated instances: At 75%RH, the perovskite structure becomes needle-like, exposing the underlying FTO and potentially creating a pathway for shunts in the eventual solar cell. Films produced using diethyl ether appear more robust, with very few pinholes visible at 50%RH, although these become more pronounced when processing at 75%RH. This is consistent with proposed mechanism of humidity resistance during spin-coating as the solubility of water in diethyl ether is significantly higher than in chlorobenzene or toluene. Ethyl acetate-produced films, on the other hand, remain remarkably continuous and consistent across the range of processing conditions, with very few visible pinholes or variation in grain sizes even at 75%RH.

Fig. 4 illustrates the effect of different anti-solvents and humidity on the crystallinity of perovskite films as determined through XRD. In Fig. 4, all patterns shown have been normalized to the height of the peak at 26.5°, corresponding to the FTO present on the glass substrate. Films processed in a N_2 glovebox across all anti-solvents exhibit relatively strong peaks at 14.04° and 28.38° corresponding to the (110) and (220) crystal planes. These peaks appear especially strong in the toluene processed film, which is in good agreement with the very large grains observed in Fig. 3 compared to films processed employing other anti-solvents during fabrication. As processing humidity is increased, however, a progressive decrease in the 14.04° peak is observed across films produced using chlorobenzene, toluene and diethyl ether. In the case of a film processed at 75%RH using diethyl ether as an anti-solvent, the peak corresponding to the (110) crystal plane is almost entirely diminished. This drop in peak intensity signals very poor crystal orientation along the stated plane. Despite a crystal-

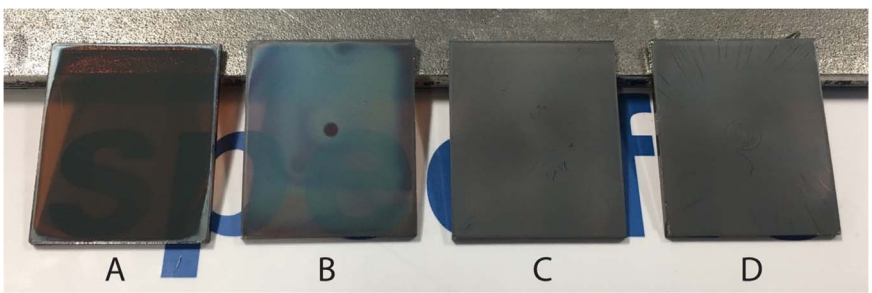

Fig. 2. Photograph of $CH_3NH_3PbI_3$ perovskite films fully processed in a 75% relative humidity environment from different anti-solvent drip routes. From left to right: (A) ethyl acetate, (B) diethyl ether, (C) toluene, (D) chlorobenzene.

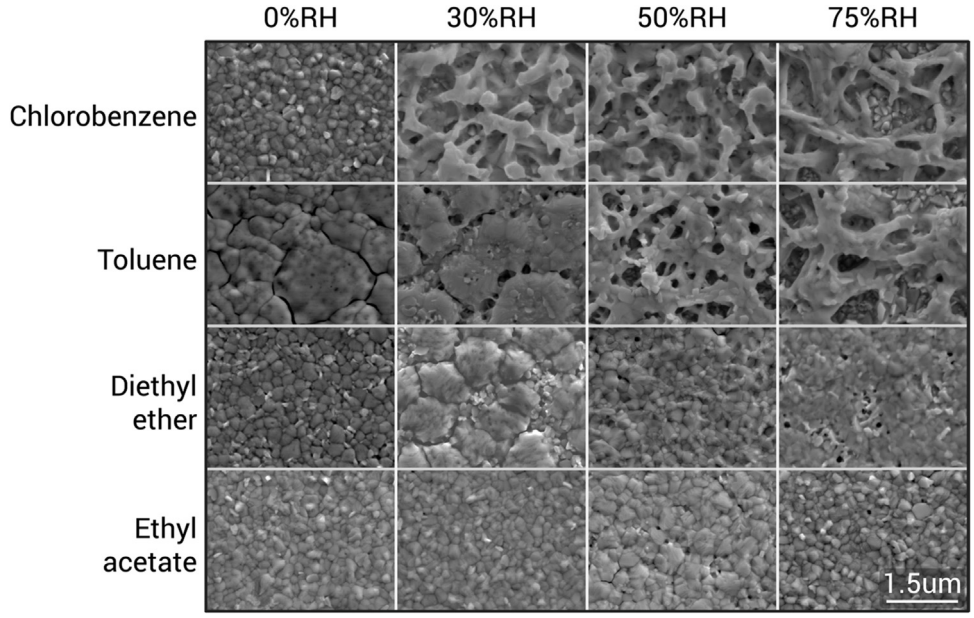

Fig. 3. Scanning electron microscopy images of $CH_3NH_3PbI_3$ perovskite films spin-coated and annealed at different relative humidities. 0%RH represents a film processed in a N_2-filled glovebox. Different anti-solvents were used to quench the perovskite precursor during spin-coating. Scale bar applies to all images.

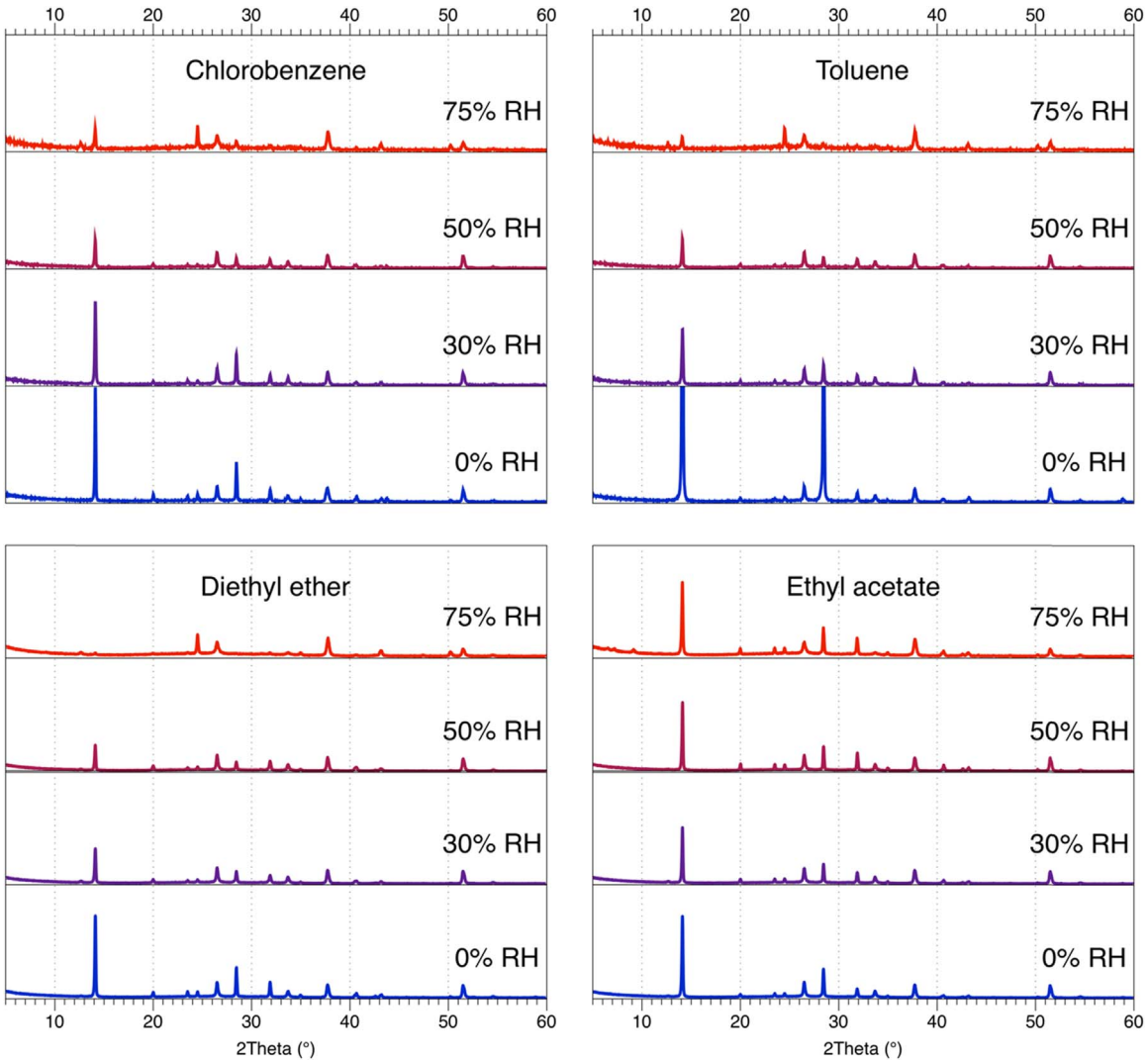

Fig. 4. XRD patterns of $CH_3NH_3PbI_3$ films processed using different anti-solvents at varying relative humidities.

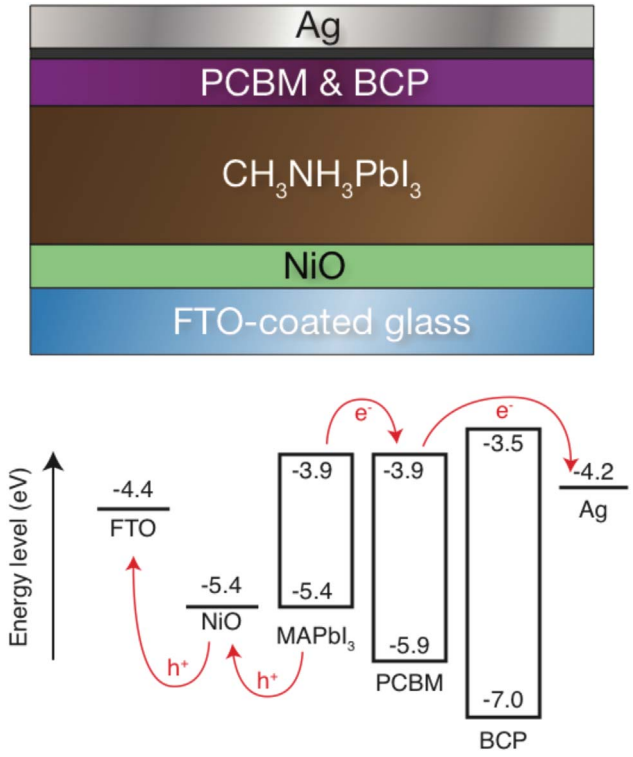

Fig. 5. Schematic and energy diagrams of the "inverted"-type solar cell architecture primarily used in this study.

linity drop when using more conventional anti-solvents, films processed using ethyl acetate exhibit almost no deterioration in peak intensity across the range of processing humidities tested. Using ethyl acetate, the peak at 14.04° is reduced by less than 7% at 75%RH compared to at 0%RH, this is in contrast with a drop of almost 80% for chlorobenzene across the same humidity range. This indicates that pinhole-free, highly crystalline and ordered perovskite films are processable under very high humidity conditions when using ethyl acetate as an anti-solvent during deposition.

2.3. High-humidity perovskite solar cell and module performance

In order to assess the impact of processing humidity on device performance, perovskite solar cells were fabricated across a range of relative humidities using a variety of anti-solvents. An inverted-type planar cell architecture, illustrated in Fig. 5, was selected so as to best challenge the fabrication process: With more conventional mesoporous layer-containing architectures, the detrimental effect pinholes within the perovskite absorber film have is somewhat mitigated by virtue of having an additional layer between charge selective contacts to block recombination. However, with a purely planar device structure, a pinhole within the perovskite represents direct contact between electron and hole transport layers; leading to a drop in device shunt resistance from increased recombination. As demonstrated further on, the most humidity-resistant processing method is applicable to a wide range of perovskite precursors and device architectures, making it highly versatile for the robust production of solar cells and perovskite films under a range of atmospheric conditions.

Fig. 6 shows averaged statistical data gathered from the J-V sweeps of solar cells. There is a clear trend towards lower PCEs with increased

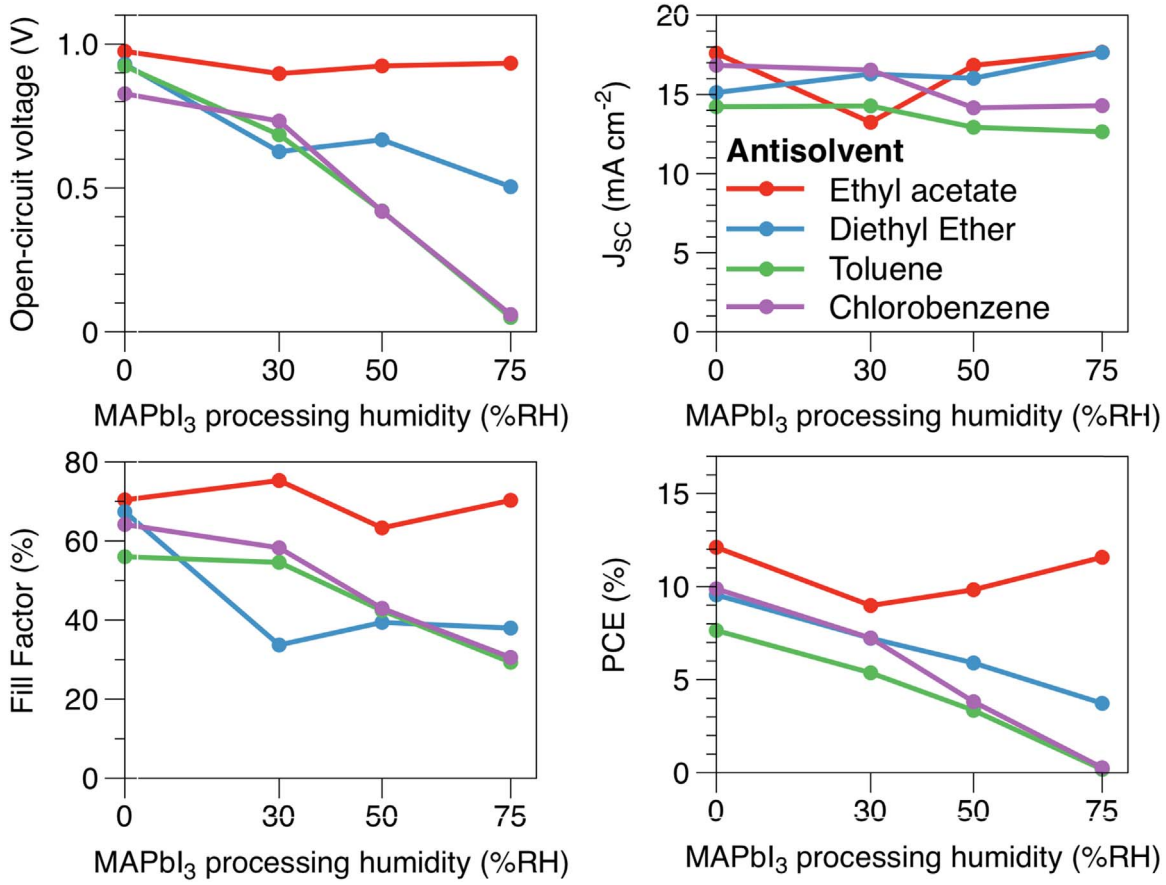

Fig. 6. Analysis of mean-average J-V characteristics for different anti-solvents at different processing humidities. A full statistical representation of J-V characteristics can be found in Figs. S3-6. Data from a total of 8 devices per variable is presented.

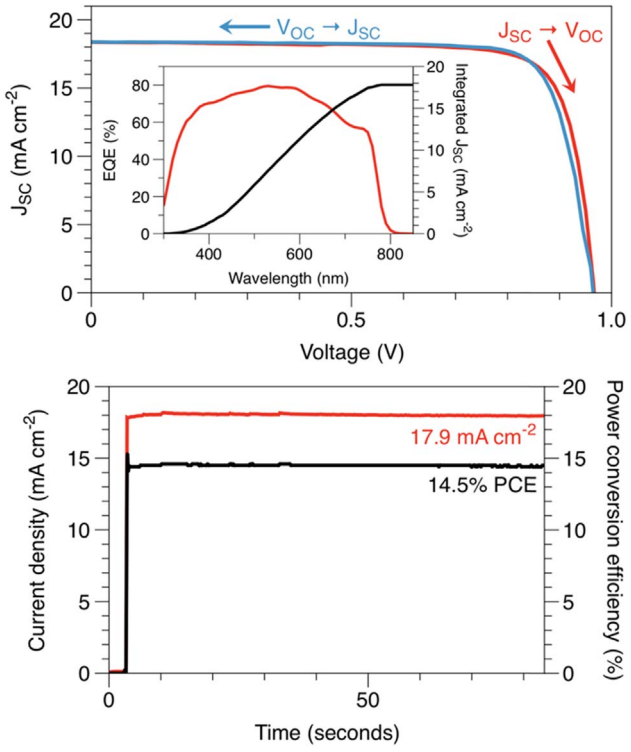

Fig. 7. J-V characteristics for the best-performing inverted-type solar cell fabricated at 75%RH. Top: Forward and reverse J-V scan, external quantum efficiency and EQE-derived current density plot. Bottom: Stabilised J_{SC} and efficiency tracking at 0.78 V.

processing humidity across the conventional anti-solvents (diethyl ether, toluene and chlorobenzene). This is primarily the result of a reduction in V_{OC} and fill factor arising from increased recombination at pinholes within the perovskite allowing contact between NiO and PCBM charge transport layers. This is confirmed in Fig. 3 which shows increasing pinhole density with processing humidity for chlorobenzene, toluene and diethyl ether anti-solvents. Devices processed using ethyl acetate, on the other hand, exhibit almost no increase in pinhole density as humidity is increased. This is reflected in the photovoltaic performance of devices, which shows far more consistently high V_{OC}, J_{SC} and fill factor across all humidities. A full report of data including box-plots for both forward and reverse J-V sweeps of all anti-solvents and humidities is shown in Figs. S2-5: A broadening of data spread is observed as humidity is increased for chlorobenzene, toluene and diethyl ether processed devices. There is also a slight increase in the variance of ethyl acetate-processed cells at 75%RH owing to more variation in fill factor and J_{SC}.

It is interesting to note that the most efficient device fabricated using any anti-solvent at any humidity was from this 75%RH batch. A full characterization of this highest performing device is shown in Fig. 7 including both forward and reverse J-V sweeps, external quantum efficiency with an estimation of the integrated J_{SC}, as well as a stabilized current and efficiency plot at the device's maximum power point. With a stabilized power conversion efficiency of 14.5%, this device represents the highest reported efficiency for a planar perovskite solar cell processed at these very high humidity ambient conditions.

When fabricating perovskite solar cells under humid ambient conditions, there exists a possibility of moisture being integrated into the perovskite film. Given the organic component of the $CH_3NH_3PbI_3$ perovskite is readily dissolved by water, there is a concern that devices processed under such “wet” conditions might suffer accelerated degra-

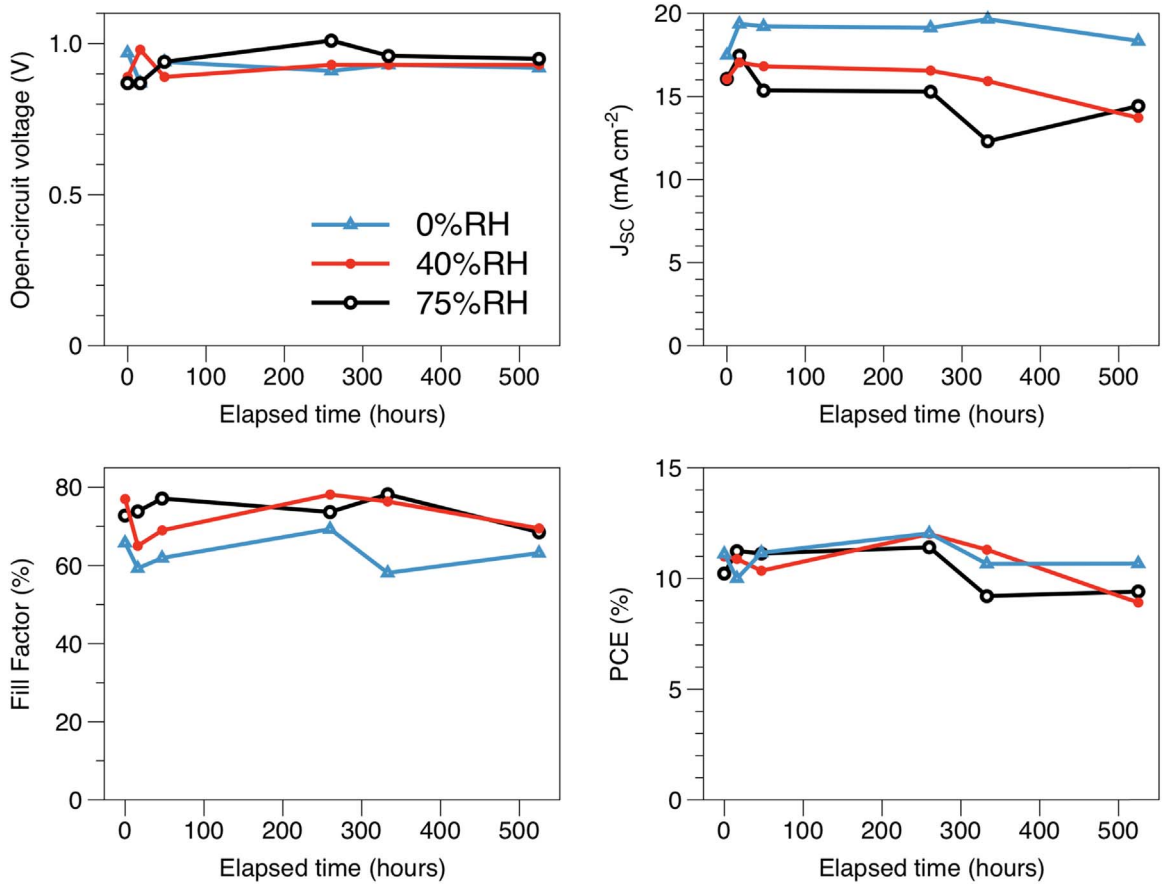

Fig. 8. Current-voltage statistics for encapsulated solar cells with perovskite processed at 0%RH, 40%RH and 75%RH over a total of 525 h. Devices were stored at open-circuit in a fluorescent light-box at 2500lx in 30%RH air.

dation compared to dry-processed counterparts. To investigate this theory, encapsulated solar cells with the same architecture as illustrated in Fig. 5. employing perovskite films produced in a dry glovebox, as well as under 40%RH and 75%RH ambient conditions were subjected to over 500 h of light exposure (2500lx, fluorescent tube) at open-circuit in air with periodic testing of J-V characteristics. The results are shown in Fig. 8. While V_{OC} remains stable over hundreds of hours for devices fabricated at different humidities, J_{SC} and fill factor tend to fluctuate to a greater degree as devices age. Nonetheless, the device with perovskite produced at 75%RH does not appear to degrade significantly faster than one fabricated entirely within a N_2-filled glovebox. This result implies that very little, if any, residual moisture is retained within the perovskite film after fabrication. However, it is also worth noting that devices underwent PCBM coating inside of a glovebox and had metallic contacts evaporated under vacuum, both of which may have removed any water from the device prior to completion.

The proposed ethyl acetate anti-solvent method for high humidity processing of perovskite films also shows remarkable uniformity over large surface areas. In order to demonstrate the extent of this consistency, a 50 mm × 50 mm sub-module was produced, comprising of 5 cells connected in series (13.5 cm^2 active area, 54% geometric fill factor). Complete fabrication was completed under 75% relative humidity conditions and outside of a dedicated cleanroom including NiO, $CH_3NH_3PbI_3$, PCBM and BCP layer deposition. A photograph of the module, as well as J-V characteristics and stabilized power-conversion efficiency measurements may be seen in Fig. 9. Despite spin-coating onto a greatly increased substrate size at high humidity, performance remains relatively high compared to 0.1 cm^2 cells, with module PCE in excess of 10% and mean-average small cell PCEs around 12% as shown in Fig. 6. Modules were also fabricated under slightly lower humidity ambient conditions, with the overall highest performing device having been processed at 50%RH yielding a stabilized PCE of 11.8% as shown in Fig. S7.

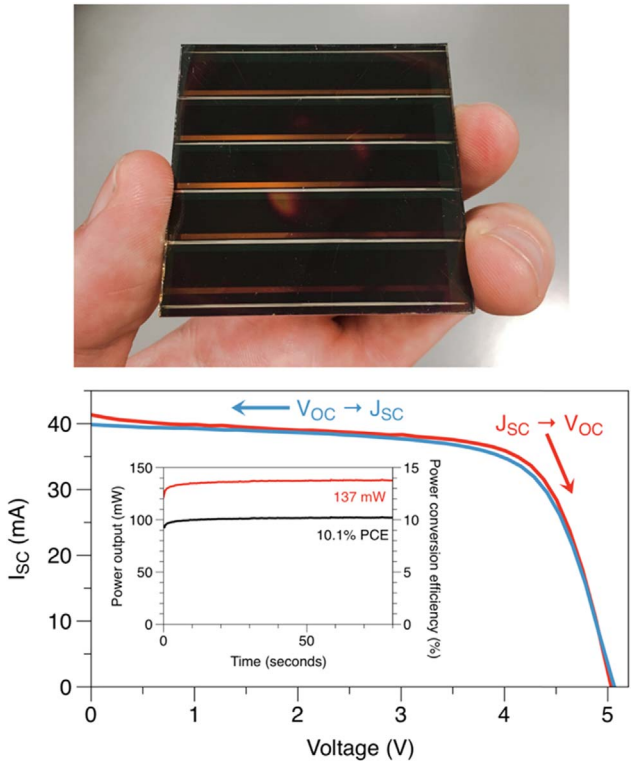

Fig. 9. Photograph, J-V characteristics and stabilised power output of a 75%RH, air-processed perovskite module employing the humidity-resistant ethyl acetate anti-solvent method. Stabilised PCE is 10.1% over an active area of 13.5 cm^2.

The effect of ethyl acetate anti-solvent processing under high ambient humidity conditions extends to multiple device architectures. In order to demonstrate the versatility of the method, devices were fabricated using an entirely different device structure: In this instance, a “normal” structure employing a mesoporous TiO_2 n-type layer combined with a spiro-OMeTAD p-type layer was used. The results, seen in Fig. 10 show a within-error variation in device performance between cells processed in a N_2-filled glovebox and in very humid air. The presence of a mesoporous TiO_2 scaffold in this architecture reduces the severity of any pinholes within the perovskite layer, thereby reducing recombination and maintaining high device performance under high humidity processing conditions. With a peak stabilized power conversion efficiency of 15% (Fig. S8), this method represents the highest efficiency perovskite solar cells processed in air at 75%RH.

3. Conclusion

We have developed a single-step spin-coating protocol able to produce high quality, pinhole-free perovskite films under very high humidity ambient conditions. The anti-solvent ethyl acetate was found to be able to sequester airborne moisture and protect the perovskite precursor's intermediate phase during spin-coating to a far greater degree than other conventional anti-solvents. Solar cells with perovskite films produced at 75%RH using this route have exhibited stabilized PCEs of 14.5% in a planar configuration and over 15% when using a mesoporous TiO_2 scaffold, showing minimal differences compared to devices produced within a N_2-filled glovebox. This robust method also yields remarkably uniform films over large areas despite a range of ambient conditions: At the same high humidity, a 50 mm × 50 mm sub-module was fabricated comprising of 5 cells connected in series with a PCE of 10.1% over an active area of 13.5 cm^2. XRD patterns and electron micrographs show consistently high quality perovskite films over a range of processing humidities for the ethyl acetate anti-solvent, compared to a deterioration in film quality as humidity is increased for a range of other commonly used anti-solvents. This processing method demonstrates the feasibility of perovskite solar cell production without the requirement for stringent atmospheric control, potentially enabling the commercial production of devices in humid climates and uncontrolled laboratories.

4. Experimental methods

4.1. Perovskite film preparation for SEM and XRD analysis

FTO-coated glass (7 Ω/sq, Solaronix) substrates were sonicated in a solution of detergent, followed by deionised water, acetone and isopropyl alcohol before undergoing 10 min of oxygen-plasma etching. A $CH_3NH_3PbI_3$ perovskite precursor solution was prepared by dissolving 576 mg PbI_2 (99%, Sigma Aldrich) and 199 mg methylammonium iodide (Dyesol) in 0.8 ml diemthylformamide (DMF) and 0.2 ml dimethyl sulfoxide (DMSO). Upon dissolution, the solution was filtered through a 0.2 μm PTFE syringe filter before use. To deposit the $CH_3NH_3PbI_3$ perovskite layer, 100 μl of the aforementioned solution was spin-coated onto FTO glass substrates at 4000 rpm for 25 s. During spin-coating, 200 μl of the desired anti-solvent was poured onto the spinning substrate 5 s prior to the end of the spin cycle. Upon completion, substrates were immediately transferred to a hotplate set within the same atmospheric environment as the spin-coater and annealed at 100 °C for 10 min.

In the case of 0%RH tests, a N_2-filled glove box was used with O_2 and H_2O content below 100 ppm and 0.5 ppm respectively. For experiments performed at 30%RH, a desiccant dehumidifier system was used to dry the air within a room. For higher relative humidity conditions, a small glove box containing both spin-coater and hotplate was purged with humidified air bubbled through a water bath. For all processing conditions, the ambient temperature was fixed at 20 °C.

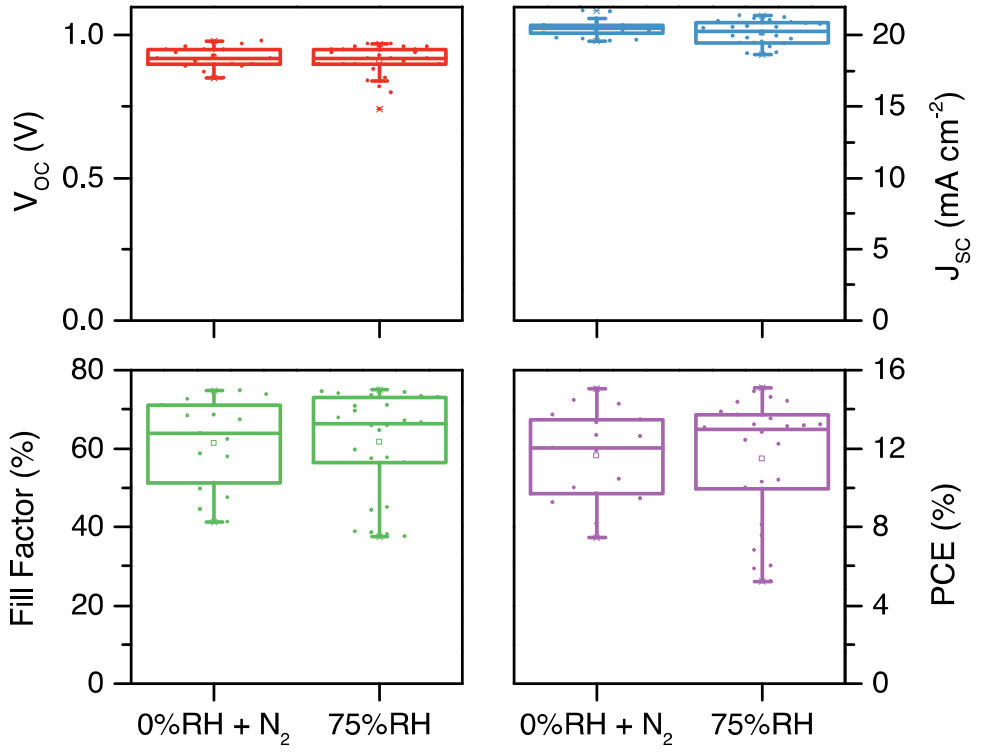

Fig. 10. J-V characteristics for perovskite solar cells fabricated using a "normal" structure employing mesoporous-TiO_2 and spiro-OMeTAD charge selective contacts. Perovskite processed inside a glovebox (0%RH + N_2) and in air with 75% relative humidity. Data from 24 devices per variable is presented.

Relative humidity was recorded using a factory calibrated sensor accurate to ± 3%RH between 0% and 80%RH (Silicon Instruments SI7021)

4.2. Inverted perovskite solar cell fabrication

To fabricate perovskite solar cells, FTO glass samples were cleaned as mentioned in Section 4.1 before being coated with a NiO hole transporting layer. This layer was spin-coated (4000 rpm, 30 s) from a 0.2 M solution of nickel acetate tetrahydrate dissolved in a 1:0.012 vol ratio of 2-methoxyethanol:ethanolamine [39]. After spin-coating, samples were annealed at 500 °C for 30 min before cooling to room temperature. $CH_3NH_3PbI_3$ perovskite layers were deposited using the method described previously. Spin-coating of $PC_{60}BM$ (20 mg/ml in chlorobenzene. 2000 rpm for 30 s) followed by bathocuproine (BCP, 0.5 mg/ml in anhydrous ethanol. 6000 rpm for 10 s) electron transport and buffer layers were performed inside a N_2-filled glovebox unless otherwise specified. 100 nm thick silver counter electrodes were evaporated at 10^{-4} Torr using an Edwards 306 thermal evaporator.

4.3. "Normal" structure perovskite solar cell fabrication

FTO glass samples were cleaned as mentioned in Section 4.1 before the deposition of a compact TiO_2 layer. A 10%vol solution of titanium diisopropoxide bis(acetylacetonate) in isopropanol was repeatedly sprayed onto FTO glass substrates at a temperature of 250 °C before undergoing a sintering process at 550 °C for 30 min. Upon cooling, a suspension of mesoporous TiO_2 nanoparticles (Dyesol 30NR-D:ethanol 2:7 wt) was spin-coated onto substrates at 4500 rpm for 30 s before re-sintering at 550 °C for 30 min. Perovskite was deposited in the same manner as described in Section 4.2. Spiro-OMeTAD was dissolved in chlorobenzene (80 mg/ml) including 30 µl/ml 4-tert-butylpyridine, 20 µl/ml bis(trifluoromethane) sulfonamide lithium salt solution (520 mg/ml in acetonitrile) and 20 µl/ml FK209-TFSI solution (300 mg/ml in acetonitrile) before being spin-coated onto the perovskite layer at 4000 rpm for 30 s. Finally, gold electrodes were evaporated at 10^{-4} Torr using an Edwards 306 thermal evaporator.

4.4. Perovskite solar module fabrication

Patterned ITO-coated glass (5 Ω/sq) was cleaned as described in Section 4.1. An identical solution of nickel acetate tetrahydrate in 2-methoxyethanol and ethanolamine (Section 4.2) was spin-coated at 4000 rpm for 30 s before annealing at 250 °C for 30 min. Subsequent perovskite and PCBM layers were processed as described in Section 4.2. A scalpel blade was used to mechanically scribe a through the PCBM, perovskite and NiO layers in order to expose the underlying ITO for series interconnection. A patterned shadow mask was used to evaporate silver electrodes connecting the anodes with cathodes for individual cells within the module.

4.5. Perovskite film characterization

Infrared spectroscopy was performed on a Perkin Elmer Spectrum 100 FT-IR spectrometer via an attenuated total reflectance (ATR) crystal. Samples were scanned with a resolution of 2 cm^{-1} over 2 accumulations. X-ray diffraction analyses of the crystalline properties of perovskite films were carried out using a Bruker D8 Discover instrument with a CuK_α beam at 40 kV and 40 mA, scan parameters of 0.1 s/step at 0.01 2θ step size. Scanning electron microscopy images of films were collected using a Jeol JSM-7800F field emission gun electron microscope with a 5 kV beam, 9 µA at approximately 10 mm working distance.

4.6. Solar cell characterization

For current-voltage measurements of solar cells, devices were masked to 0.1 cm^2 and tested under a class AAA solar simulator (Newport Oriel Sol3A) at AM1.5 and 100 mW cm^{-2} illumination conditions calibrated against a KG5 filtered silicon reference cell

(Newport Oriel 91150-KG5) using a Keithley 2400 source meter. Current-voltage sweeps were performed from both V_{OC}-to-J_{SC} and vice versa at a rate of 0.1 V s^{-1}. For stabilized power output measurements, device bias was set to the maximum power point voltage determined by the J-V sweep and current monitored under 100 mW cm^{-2} illumination. External quantum efficiency measurements were performed in 10 nm increments on a PV Measurements QEX10 in DC mode calibrated against a NIST-traceable photodiode.

Acknowledgements

The authors would like to acknowledge the support provided from the Engineering and Physical Sciences Research Council (EPSRC) through the Self-assembling Perovskite Absorbers – Cells Engineered into Modules project (EP/M015254/1) and the SPECIFIC Innovation and Knowledge Centre (EP/N020863/1). The authors would also like to express their gratitude to the Welsh Government for their support of the Sêr Solar programme.

Appendix A. Supporting information

Supplementary data associated with this article can be found in the online version at doi:10.1016/j.nanoen.2017.06.039.

References

[1] A. Kojima, K. Teshima, Y. Shirai, T. Miyasaka, Organometal halide perovskites as visible-light sensitizers for photovoltaic cells, J. Am. Chem. Soc. 131 (2009) 6050–6051.
[2] M.M. Lee, J. Teuscher, T. Miyasaka, T.N. Murakami, H.J. Snaith, Efficient hybrid solar cells based on meso-superstructured organometal halide perovskites, Science (80-.) 338 (2012) 643–647.
[3] H.-S. Kim, C.-R. Lee, J.-H. Im, K.-B. Lee, T. Moehl, A. Marchioro, S.-J. Moon, R. Humphry-Baker, J.-H. Yum, J.E. Moser, M. Gratzel, N.-G. Park, Lead iodide perovskite sensitized all-solid-state submicron thin film mesoscopic solar cell with efficiency exceeding 9%, Sci. Rep. (2012).
[4] M. Grätzel, The light and shade of perovskite solar cells, Nat. Mater. 13 (2014) 838–842.
[5] N.-G. Park, Crystal growth engineering for high efficiency perovskite solar cells, CrystEngComm 18 (2016) 5977–5985.
[6] S.D. Stranks, G.E. Eperon, G. Grancini, C. Menelaou, M.J.P. Alcocer, T. Leijtens, L.M. Herz, A. Petrozza, H.J. Snaith, Electron-hole diffusion lengths exceeding 1 μm in an organometal trihalide perovskite absorber, Science (80-.) 342 (2013) 341–344.
[7] G.E. Eperon, S.D. Stranks, C. Menelaou, M.B. Johnston, L.M. Herz, H.J. Snaith, Formamidinium lead trihalide: a broadly tunable perovskite for efficient planar heterojunction solar cells, Energy Environ. Sci. 7 (2014) 982–988.
[8] J. Burschka, N. Pellet, S.-J. Moon, R. Humphry-Baker, P. Gao, M.K. Nazeeruddin, M. Gratzel, Sequential deposition as a route to high-performance perovskite-sensitized solar cells, Nature 499 (2013) 316–319.
[9] M. Liu, M.B. Johnston, H.J. Snaith, Efficient planar heterojunction perovskite solar cells by vapour deposition, Nature 501 (2013) 395–398.
[10] Q. Chen, H. Zhou, Z. Hong, S. Luo, H.-S. Duan, H.-H. Wang, Y. Liu, G. Li, Y. Yang, Planar heterojunction perovskite solar cells via vapor-assisted solution process, J. Am. Chem. Soc. 136 (2013) 622–625.
[11] O. Malinkiewicz, A. Yella, Y.H. Lee, G.M. Espallargas, M. Graetzel, M.K. Nazeeruddin, H.J. Bolink, Perovskite solar cells employing organic charge-transport layers, Nat. Photonics 8 (2014) 128–132.
[12] H.S. Kim, I.H. Jang, N. Ahn, M. Choi, A. Guerrero, J. Bisquert, N.G. Park, Control of I-V hysteresis in CH3NH3PbI3 perovskite solar cell, J. Phys. Chem. Lett. 6 (2015) 4633–4639.
[13] J.H. Noh, S.H. Im, J.H. Heo, T.N. Mandal, S. Il Seok, Chemical management for colorful, efficient, and stable inorganic-organic hybrid nanostructured solar cells, Nano Lett. 13 (2013) 1764–1769.
[14] G. Niu, W. Li, F. Meng, L. Wang, H. Dong, Y. Qiu, Study on the stability of CH3NH3PbI3 films and the effect of post-modification by aluminum oxide in all-solid-state hybrid solar cells, J. Mater. Chem. A 2 (2014) 705.
[15] Z. Song, A. Abate, S.C. Watthage, G.K. Liyanage, A.B. Phillips, U. Steiner, M. Graetzel, M.J. Heben, Perovskite solar cell stability in humid air: partially reversible phase transitions in the PbI2-CH3NH3I-H2O system, Adv. Energy Mater. 6 (2016) 1600846.
[16] J. Yang, B.D. Siempelkamp, D. Liu, T.L. Kelly, Investigation of CH3NH3PbI3 degradation rates and mechanisms in controlled humidity environments using in situ techniques, ACS Nano 9 (2015) 1955–1963.
[17] H.-S. Ko, J.-W. Lee, N.-G. Park, 15.76% efficiency perovskite solar cells prepared under high relative humidity: importance of PbI2 morphology in two-step deposition of CH3NH3PbI3, J. Mater. Chem. A 3 (2015) 8808–8815.
[18] H. Zhou, Q. Chen, G. Li, S. Luo, T.-B. Song, H.-S. Duan, Z. Hong, J. You, Y. Liu, Y. Yang, Interface engineering of highly efficient perovskite solar cells, Science (80-.) 345 (2014) 542–546.
[19] J. Xu, Z. Hu, X. Jia, L. Huang, X. Huang, L. Wang, P. Wang, H. Zhang, J. Zhang, J. Zhang, Y. Zhu, A rapid annealing technique for efficient perovskite solar cells fabricated in air condition under high humidity, Org. Electron. Phys. Mater. Appl. 34 (2016) 84–90.
[20] B. Lei, V.O. Eze, T. Mori, High-performance CH3NH3PbI3 perovskite solar cells fabricated under ambient conditions with high relative humidity, Jpn. J. Appl. Phys. 54 (2015).
[21] G. Sfyri, C.V. Kumar, D. Raptis, V. Dracopoulos, P. Lianos, Study of perovskite solar cells synthesized under ambient conditions and of the performance of small cell modules, Sol. Energy Mater. Sol. Cells 134 (2015) 60–63.
[22] P. Luo, Z. Liu, W. Xia, C. Yuan, J. Cheng, Y. Lu, Uniform, stable, and efficient planar-heterojunction perovskite solar cells by facile low-pressure chemical vapor deposition under fully open-air conditions, ACS Appl. Mater. Interfaces 7 (2015) 2708–2714.
[23] S.R. Raga, M.C. Jung, M.V. Lee, M.R. Leyden, Y. Kato, Y. Qi, Influence of air annealing on high efficiency planar structure perovskite solar cells, Chem. Mater. 27 (2015) 1597–1603.
[24] M.K. Gangishetty, R.W.J. Scott, T.L. Kelly, Effect of relative humidity on crystal growth, device performance and hysteresis in planar heterojunction perovskite solar cells, Nanoscale 3 (2015) 6300–6307.
[25] Q. Tai, P. You, H. Sang, Z. Liu, C. Hu, L.W. Helen, Efficient and stable perovskite solar cells prepared in ambient air irrespective of the humidity, Nat. Commun. 6 (2016) 1–8.
[26] J.W. Lee, H.S. Kim, N.G. Park, Lewis acid-base adduct approach for high efficiency perovskite solar cells, Acc. Chem. Res. 49 (2016) 311–319.
[27] N.J. Jeon, J.H. Noh, Y.C. Kim, W.S. Yang, S. Ryu, S. Il Seok, Solvent engineering for high-performance inorganic-organic hybrid perovskite solar cells, Nat. Mater. 13 (2014) 1–7.
[28] M. Xiao, F. Huang, W. Huang, Y. Dkhissi, Y. Zhu, J. Etheridge, A. Gray-Weale, U. Bach, Y.B. Cheng, L. Spiccia, A fast deposition-crystallization procedure for highly efficient lead iodide perovskite thin-film solar cells, Angew. Chem. – Int. Ed. 53 (2014) 9898–9903.
[29] M. Saliba, T. Matsui, J.-Y. Seo, K. Domanski, J.-P. Correa-Baena, M.K. Nazeeruddin, S.M. Zakeeruddin, W. Tress, A. Abate, A. Hagfeldt, M. Grätzel, Cesium-containing triple cation perovskite solar cells: improved stability, reproducibility and high efficiency, Energy Environ. Sci. 9 (2016) 1989–1997.
[30] F. Giordano, A. Abate, J. Pablo, C. Baena, M. Saliba, T. Matsui, S.H. Im, S.M. Zakeeruddin, M.K. Nazeeruddin, A. Hagfeldt, M. Graetzel, Enhanced electronic properties in mesoporous TiO2 via lithium doping for high-efficiency perovskite solar cells, Nat. Commun. 7 (2016) 1–6.
[31] M. Yin, F. Xie, H. Chen, X. Yang, F. Ye, E. Bi, Y. Wu, M. Cai, L. Han, Annealing-free perovskite films by instant crystallization for efficient solar cells, J. Mater. Chem. A 4 (2016) 8548–8553.
[32] J.W. Jung, S.T. Williams, A.K.-Y. Jen, Low-temperature processed high-performance flexible perovskite solar cells via rationally optimized solvent washing treatments, RSC Adv. 4 (2014) 62971–62977.
[33] V. Ferreira, L. Ortega, A. Escudero, J.F. Cacho, A comparative study of the ability of different solvents and adsorbents to extract aroma compounds from alcoholic beverages, J. Chromatogr. Sci. 38 (2000) 469–476.
[34] H.H. Rowley, W.R. Reed, Solubility of water in diethyl ether at 25 dC, J. Am. Chem. Soc. 73 (1951) 2960.
[35] K. László, B. Demé, O. Czakkel, E. Geissler, Incompatible liquids in confined conditions, J. Phys. Chem. C 118 (2014) 23723–23727.
[36] S. Mitra, Sample Preparation Techniques in Analytical Chemistry, 2003.
[37] T. Baikie, Y. Fang, J.M. Kadro, M. Schreyer, F. Wei, S.G. Mhaisalkar, M. Graetzel, T.J. White, Synthesis and crystal chemistry of the hybrid perovskite (CH3NH3) PbI3 for solid-state sensitised solar cell applications, J. Mater. Chem. A 1 (2013) 5628–5641.
[38] G.E. Eperon, S.N. Habisreutinger, T. Leijtens, B.J. Bruijnaers, J.J. Van, R.A.J. Janssen, A. Petrozza, H.J. Snaith, The importance of moisture in hybrid lead halide perovskite thin film fabrication, ACS Nano (2015) 9380–9393.
[39] S. Wheeler, F. Deledalle, N. Tokmoldin, T. Kirchartz, J. Nelson, J.R. Durrant, Influence of surface recombination on charge-carrier kinetics in organic bulk heterojunction solar cells with nickel oxide interlayers, Phys. Rev. Appl. 4 (2015) 24020.